Efficient gas-phase generation of coherent vacuum ultraviolet radiation

Andrew J. Merriam, S. J. Sharpe, H. Xia, D. Manuszak, G. Y. Yin, and S. E. Harris

Edward L. Ginzton Laboratory, Stanford University, Stanford, California 94305

Received February 1, 1999

We report the demonstration of a pulsed atomic lead (Pb) vapor-based vacuum ultraviolet frequency converter from 233 to 186 nm with unity photon-conversion efficiency. This conversion is attained without phase matching. © 1999 Optical Society of America

OCIS codes: 190.2620, 190.4410, 270.1670, 020.1670, 190.7220, 190.4380.

The techniques of electromagnetically induced transparency (EIT) can be employed to create a nonlinear response at a given wavelength that is equal in magnitude to the linear response at that wavelength. Physically, this allows frequency converters wherein unity photon-to-photon conversion occurs within a single coherence length, i.e., in that distance that causes a π phase slip between the driving polarization and the generated electromagnetic wave. These ideas were first implemented by Jain and co-workers[1] to convert 425 nm to 293 nm with an energy conversion efficiency of 40%, in a medium consisting of a single isotope of Pb. The enhancement of nonlinear optical processes using EIT has driven much recent theoretical[2] and experimental[3,4] work.

This Letter reports the demonstration of a vapor-phase vacuum ultraviolet frequency converter from 233 to 186 nm with unity photon conversion efficiency. Up to 300 μJ of 186 nm is generated, with a peak power of 25 kW.

Our technique is this: two strong pulsed laser fields (MW/cm^2-class) are applied that are two-photon resonant with a Raman transition of the Pb atoms, as shown in the inset of Fig. 1. Similar to previous EIT work,[5] a 283-nm probe laser and a 406-nm coupling laser adiabatically drive all the atoms of the ensemble into a maximally coherent superposition of the ground and metastable states. Following the level designations of Fig. 1, maximal coherence of the Raman ($|1\rangle \rightarrow |2\rangle$) transition is defined as the condition in which the density matrix elements satisfy $\rho_{11} = \rho_{22} = |\rho_{12}| = 1/2$. Once the atoms are driven to this dark state, they are decoupled from the applied optical fields, and, hence, the high-intensity probe and coupling lasers maintain wave vectors equal to their vacuum values and propagate without loss or distortion.[6] This permits substantial resonant enhancement of the four-wave-mixing nonlinear optical susceptibilities that govern the generation of the upconverted radiation. The atomic coherence, ρ_{12}, acts as a local oscillator and a third applied frequency beats against it to produce sum and difference frequencies. This frequency converter has the special property that, when the atoms of the ensemble are driven at maximal coherence, 100% of the input photons may be upconverted within a single coherence length, thus obviating the need to phase match the propagating beams.

This experiment has been carried out in natural-abundance Pb metal at a density–length NL product of 1.5×10^{17} atoms/cm^2, under conditions where the transmission of a resonant weak-probe 283-nm beam, if alone, would be approximately $\exp(-2 \times 10^5)$. Natural abundance Pb consists of three isotopes, 24% ^{206}Pb, 23% ^{207}Pb, and 53% ^{208}Pb. Of the three, the ^{207}Pb isotope has a nonzero nuclear angular momentum and therefore displays hyperfine structure. To establish the dark superposition state in this hyperfine-structure-split isotope, the probe and the coupling lasers must be tuned to the centers of gravity of the hyperfine-split transitions, which, to within a small isotopic shift, coincide with the level positions in the unsplit isotopes. In addition, the coupling laser Rabi frequency must exceed the hyperfine splitting. These concepts were detailed and demonstrated by Xia *et al.*[7]

The experimental setup is shown in Fig. 1. Three strong, linearly polarized, coherent beams at 406, 283, and 233 nm are combined by BC1 and BC2, converted to circular polarization by a Fresnel rhomb (FR), and propagate collinearly through the Pb atomic vapor generated in a heat pipe (HP). The output beams are dispersed by a Pellin–Broca prism (PB), and the

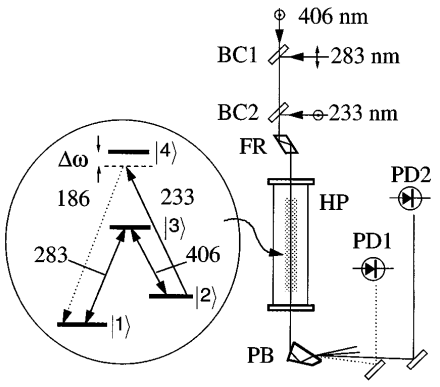

Fig. 1. Schematic diagram of the experimental setup and energy-level diagram for atomic Pb. Level assignments: $|1\rangle$, $6p^2\,{}^3P_0$ (ground); $|2\rangle$, $6p^2\,{}^3P_2$; $|3\rangle$, $6p7s\,{}^3P_1$; and $|4\rangle$, $6p9s\,{}^3P_1$. Hyperfine structure is not shown. The probe laser at 283 nm and coupling laser at 406 nm have opposite circular polarizations and prepare a large atomic coherence; the mixing field at 233 nm has the same-sense circular polarization as the coupling laser and mixes with the coherence to generate a sum frequency at 186 nm. BC1, BC2, beam combiners.

0146-9592/99/090625-03$15.00/0

generated field at 186 nm and the residual mixing field at 233 nm are sampled by fast windowless Si photodiodes PD1 and PD2, respectively. The output 283-nm beam quality, which is an indication of the quality of the EIT, is monitored in real time by a CCD camera. The input and output waveforms are connected to a 5-Gsample/s Tektronix TDS 684A four-channel, real-time digitizing oscilloscope controlled by a computer. This system downloads the digitized waveforms on a shot-by-shot basis. The data are later analyzed, sorted by the pulse timing, and plotted. Because each laser system is pumped by independent frequency-doubled Nd:YAG sources, there is $\approx \pm 10$ ns of jitter between the various pulses. Data with pulse timing overlap errors of less than 5 ns are retained (approximately 10% of the total number of laser shots). The data shown in Figs. 2 and 3 are from individual events and are not averaged.

The Pb metal vapor for the experiment is produced within a 1-in.-diameter 3-ft-long type-316 stainless-steel heat pipe employing a stainless-steel mesh wick, which may be heated to temperatures up to 1200 °C by concentric Mb heaters in a vacuum oven. Varying the Xe buffer-gas pressure between 2 and 8 Torr provides Pb metal-vapor densities of 1×10^{16} to 5×10^{16} atoms/cm^3, with a typical metal-vapor zone length of 1 to 10 cm.

The applied coherent fields for the experiment are pulsed, with Fourier-transform-limited bandwidths. The laser setup is similar to that used in previous experiments.[1,8] The coupling laser is obtained by means of frequency doubling the output of a single-longitudinal-mode injection-seeded pulsed Ti:sapphire laser oscillator operating at 812 nm. This system generates up to 20 mJ of 406 nm with a 30-ns pulse width. The probe laser is obtained by frequency tripling the output of a similar laser system operating at 850 nm, which generates up to 3 mJ/pulse of 283 nm and a 15-ns pulse width.[9] Up to 1 mJ/pulse of the mixing field at 233 nm (pulse width 12–15 ns) is obtained by frequency tripling the output of a widely tunable self-seeding single-longitudinal-mode, Ti:sapphire laser operating at 700 nm.[10] The frequencies of the lasers are determined using a Burleigh Model 4500 pulsed wavemeter with a maximum resolution of 0.01 cm^{-1} (300 MHz). The beam areas of the 406-nm coupling laser, 283-nm probe laser, and 233-nm mixing beam at the center of the vapor zone (calculated from the intensity full-width-at-$1/e^2$ points), are 3.3, 0.6, and 0.15 mm^2, respectively. The area of the generated beam is inferred to be the same as that of the 233-nm mixing beam. Typical energies and Rabi frequencies in the 6-cm vapor zone for the probe, coupling, mixing, and generated lasers are 800 μJ (3.5 cm^{-1}), 12 mJ (7.0 cm^{-1}), 200 μJ (1.0 cm^{-1}), and 200 μJ (1.1 cm^{-1}), respectively. These Rabi frequencies are calculated for circular polarizations of appropriate handedness using weighted oscillator strengths, gf, of 0.197, 0.028, and 0.027, respectively.

The generated 186-nm vacuum ultraviolet signal is monitored by a windowless Si photodiode (PD1) that has been calibrated by a Molectron pyroelectric joulemeter (Model J4-09), and the measured energy is corrected for the attenuation of the various optics and for 50-cm propagation through air. At this wavelength, the dominant absorber in air is water vapor; at 20 °C and a relative humidity of 40%, the measured attenuation coefficient of air is $\approx$1.5%/cm. The overall attenuation is approximately −11 dB from the source (inside the heat pipe) to the detector.

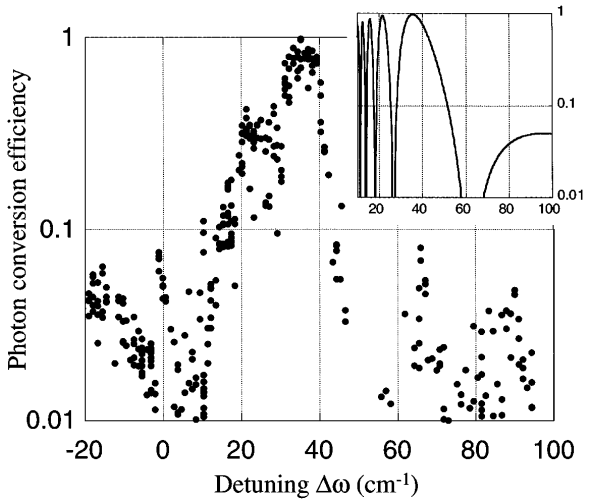

Fig. 2. Photon-conversion efficiency from the applied 233-nm mixing beam to the generated 186-nm beam as a function of the detuning $\Delta\omega$ from the upper $6p9s\,^3P_1$ level. Inset: calculated conversion efficiency. The Pb metal density–length product for these data is 1.5×10^{17} atoms/cm^2.

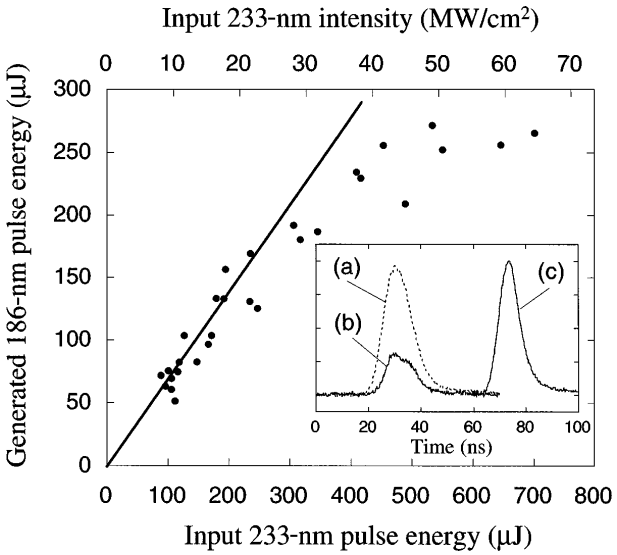

Fig. 3. Saturation behavior and depletion in the 186-nm FWM process at a detuning of 40 cm^{-1} below the $6p9s\,^3P_1$ resonance. The generated 186-nm energy increases linearly with the applied 233-nm energy, indicating constant small-signal conversion efficiency ($\approx$70%, as indicated by the solid line) and then saturates. Inset: recorded waveforms showing depletion of the 233-nm mixing field. (a) 233-nm mixing field at the exit of the heat pipe when the probe and the coupling lasers are blocked (no conversion). When significant generation occurs, the 233-nm field at the exit is depleted (b), and the 186-nm beam is generated (c). Trace (c) has been normalized and shifted from the other curves for better perspective.

In Fig. 2 we show the photon conversion efficiency from 233 to 186 nm as a function of the detuning of the 233-nm mixing beam from the $6p9s\,^3P_1$ level. The photon conversion efficiency reaches a maximum of 98% ± 10% at a detuning of 35 cm^{-1} and then decreases in a series of oscillations to near zero at 5-cm^{-1} detuning. The conversion then increases to approximately 8% when both beams are resonant with the $6p9s\,^3P_1$ level. For these data, the frequencies of the probe and coupling lasers are set at values that optimize the transmission of the strong-probe lasers *in the absence of the mixing and generated beams* and are held constant throughout the course of the data run. No attempt is made to optimize the generated signal by adjusting the wave vector of the atomic coherence through two-photon detuning. The probe laser and the coupling laser peak Rabi frequencies are 3.5 and 7.0 cm^{-1}, respectively, which establishes a near-maximal coherence $\rho_{12} = -0.4$. At peak photon converter efficiency, the net energy conversion efficiency to 186 nm, including all three beams, irrespective of beam overlap factors, is roughly 2%. This is by no means a fundamental limit; in the present experiment, the establishment of a central region of spatially homogeneous atomic coherence using Gaussian probe and coupling beams requires large beam sizes and, consequently, extra energy. The net efficiency can be increased by using smaller, flat-top optical beams.

In Fig. 3 we show the saturation behavior of the frequency converter at a detuning of 40 cm^{-1} below the $6p9s\,^3P_1$ resonance. The solid line indicates 70% small-signal energy conversion; above a mixing field intensity of ~25 MW/cm^2, the conversion efficiency saturates and is reduced significantly below the small-signal value. The saturation is due to energy depletion of the 283-nm probe laser and the A.C. Stark shift of state $|2\rangle$ as caused by the strong 233-nm mixing field. At this detuning the 2-cm^{-1} Rabi frequency of the 233-nm field causes a 0.025-cm^{-1} downward light shift, which is on a scale with that of two-photon detuning, which causes severe distortions of the strong probe laser in the absence of the mixing beam. Partial compensation for the light shift is possible by detuning and (or) chirping of the probe and coupling lasers, which may aid in extending the range of linear conversion efficiency.

At large conversion efficiencies one would expect substantial depletion of the applied 233-nm beam. As shown in the inset of Fig. 3, under conditions of 61% photon (76% energy) conversion efficiency, this is indeed the case. The ratio of the 233-nm photodiode signals at the entrance and the exit of the heat pipe yields the fractional photon loss and hence a measure of the conversion efficiency; this conversion efficiency agrees well with that calculated from the measured 186-nm energy. Additionally, as observed on a CCD camera, the applied, depleted 233-nm, and generated 186-nm beams have Gaussian spatial profiles, implying near-uniform conversion.

The coupled differential equations describing a plane-wave, small-signal frequency converter, and their solutions, are detailed in Ref. 1. At an NL product of 1.5×10^{17} atoms/cm^2, the first unity conversion point is expected to occur at a detuning of 136 cm^{-1}. The data of Fig. 2 indicate that the point of maximum conversion occurs much closer to the line center, at a detuning of 35 cm^{-1}. Suppression and shifting of the first conversion-efficiency peak are most likely caused by an additional phase mismatch induced by off-resonant transitions. The inset of Fig. 2 shows the solution of Eq. (4) of Ref. 1 for these experimental parameters with an additional (constant) phase mismatch $\Delta kL = 2\pi$. The spread in conversion efficiency data for $\Delta\omega > 60$ cm^{-1} is caused by fluctuations in Δk that are due to unintended, small shot-to-shot changes in the probe and the coupling laser frequencies and temporal overlaps. We note that our choice of optical field polarization prevents the difference-frequency-generation process that would otherwise generate a field at 42 860−10 650 $cm^{-1} \approx 310$ nm.

In summary, we have described an atomic-vapor-based frequency upconverter from 233 to 186 nm with up to unity photon conversion. Energy is parametrically transferred between the fields in a periodic fashion as the applied 233-nm field is tuned to the upper $6p9s\,^3P_1$ resonance. The resulting oscillations in conversion efficiency were observed experimentally, in agreement with small-signal plane-wave predictions. Energy depletion of the applied 233-nm mixing field was observed by use of photodiode waveforms and CCD camera images. The technique described above should allow the extension of gas-phase coherent sources to spectral regions that are well beyond the transparency regions of crystalline media.

The authors thank P. T. Epp and R. Burnham for assistance with the heat-pipe preparation, which permitted long-term high-fluence operation. This work was supported by the U.S. Army Research Office, the U.S. Office of Naval Research, and the U.S. Air Force Office of Scientific Research.

References

1. M. Jain, H. Xia, G. Y. Yin, A. J. Merriam, and S. E. Harris, Phys. Rev. Lett. **77,** 4326 (1996); S. E. Harris, G. Y. Yin, M. Jain, H. Xia, and A. J. Merriam, Philos. Trans. R. Soc. London Ser. A **355,** 2291 (1997).
2. M. D. Lukin, P. Hemmer, M. Loffler, and M. O. Scully, Phys. Rev. Lett. **81,** 2675 (1998).
3. K. Hakuta, L. Marmet, and B. P. Stoicheff, Phys. Rev. Lett. **66,** 596 (1991); see also L. Deng, W. R. Garrett, M. G. Payne, and D. Z. Lee, Opt. Lett. **21,** 928 (1996).
4. P. Hemmer, D. Katz, J. Donoghue, M. Cronin-Golomb, M. Shahriar, and P. Kumar, Opt. Lett. **20,** 982 (1995).
5. S. E. Harris, Phys. Today **50**(7), 36 (1997).
6. M. Jain, A. J. Merriam, A. Kasapi, G. Y. Yin, and S. E. Harris, Phys. Rev. Lett. **75,** 4385 (1995).
7. H. Xia, S. J. Sharpe, A. J. Merriam, and S. E. Harris, Phys. Rev. A **56,** R3362 (1997); H. Xia, A. J. Merriam, S. J. Sharpe, and S. E. Harris, "Electromagnetically induced transparency with spectator momenta," Phys. Rev. A (to be published).
8. A. Kasapi, M. Jain, G. Y. Yin, and S. E. Harris, Phys. Rev. Lett. **74,** 2447 (1995).
9. A. Kasapi, M. Jain, and G. Y. Yin, Appl. Phys. Lett. **35,** 1999 (1996).
10. A. J. Merriam and G. Y. Yin, Opt. Lett. **23,** 1034 (1998).